Coherent x-ray zoom condenser lens for diffractive and scanning microscopy

Takashi Kimura,[1,2] Satoshi Matsuyama,[2,3] Kazuto Yamauchi,[2,3,4] and Yoshinori Nishino[1,2,*]

[1]*Research Institute for Electronic Science, Hokkaido University, Kita 21 Nishi 10, Kita-ku, Sapporo 001-0021, Japan*
[2]*Japan Science and Technology Agency, CREST, 4-1-8 Honcho, Kawaguchi, Saitama 332-0012, Japan*
[3]*Department of Precision Science and Technology, Graduate School of Engineering, Osaka University, 2-1 Yamada-oka, Suita, Osaka 565-0871, Japan*
[4]*Center for Ultra-Precision Science and Technology, Graduate School of Engineering, Osaka University, 2-1 Yamada-oka, Suita, Osaka 565-0871, Japan*
[*]*yoshinori.nishino@es.hokudai.ac.jp*

Abstract: We propose a coherent x-ray zoom condenser lens composed of two-stage deformable Kirkpatrick-Baez mirrors. The lens delivers coherent x-rays with a controllable beam size, from one micrometer to a few tens of nanometers, at a fixed focal position. The lens is suitable for diffractive and scanning microscopy. We also propose non-scanning coherent diffraction microscopy for extended objects by using an apodized focused beam produced by the lens with a spatial filter. The proposed apodized-illumination method will be useful in highly efficient imaging with ultimate storage ring sources, and will also open the way to single-shot coherent diffraction microscopy of extended objects with x-ray free-electron lasers.

OCIS codes: (340.7470) X-ray mirrors; (340.7460) X-ray microscopy; (100.5070) Phase retrieval.

References and links

1. A. Sakdinawat and D. Attwood, "Nanoscale X-ray imaging," Nat. Photonics **4**(12), 840–848 (2010).
2. G. E. Ice, J. D. Budai, and J. W. L. Pang, "The race to x-ray microbeam and nanobeam science," Science **334**(6060), 1234–1239 (2011).
3. R. Falcone, C. Jacobsen, J. Kirz, S. Marchesini, D. Shapiro, and J. Spence, "New directions in X-ray microscopy," Contemp. Phys. **52**(4), 293–318 (2011).
4. J. Miao, P. Charalambous, J. Kirz, and D. Sayre, "Extending the methodology of X-ray crystallography to allow imaging of micrometre-sized non-crystalline specimens," Nature **400**(6742), 342–344 (1999).
5. I. K. Robinson and R. Harder, "Coherent X-ray diffraction imaging of strain at the nanoscale," Nat. Mater. **8**(4), 291–298 (2009).
6. J. Pérez and Y. Nishino, "Advances in X-ray scattering: from solution SAXS to achievements with coherent beams," Curr. Opin. Struct. Biol. **22**(5), 670–678 (2012).
7. R. Mokso, P. Cloetens, E. Maire, W. Ludwig, and J.-Y. Buffière, "Nanoscale zoom tomography with hard x rays using Kirkpatrick-Baez optics," Appl. Phys. Lett. **90**(14), 144104 (2007).
8. K. Shinohara, A. Ito, H. Nakano, I. Kodama, T. Honda, T. Matsumura, and K. Kinoshita, "X-ray holographic microscopy of biological specimens with an electronic zooming tube," J. Synchrotron Radiat. **3**(1), 35–40 (1996).
9. I. K. Robinson, F. Pfeiffer, I. A. Vartanyants, Y. Sun, and Y. Xia, "Enhancement of coherent X-ray diffraction from nanocrystals by introduction of X-ray optics," Opt. Express **11**(19), 2329–2334 (2003).
10. C. G. Schroer, P. Boye, J. M. Feldkamp, J. Patommel, A. Schropp, A. Schwab, S. Stephan, M. Burghammer, S. Schöder, and C. Riekel, "Coherent X-Ray diffraction imaging with nanofocused illumination," Phys. Rev. Lett. **101**(9), 090801 (2008).
11. Y. Takahashi, Y. Nishino, R. Tsutsumi, H. Kubo, H. Furukawa, H. Mimura, S. Matsuyama, N. Zettsu, E. Matsubara, T. Ishikawa, and K. Yamauchi, "High-resolution diffraction microscopy using the plane-wave field of a nearly diffraction limited focused x-ray beam," Phys. Rev. B **80**(5), 054103 (2009).
12. H. Mimura, S. Handa, T. Kimura, H. Yumoto, D. Yamakawa, H. Yokoyama, S. Matsuyama, K. Inagaki, K. Yamamura, Y. Sano, K. Tamasaku, Y. Nishino, M. Yabashi, T. Ishikawa, and K. Yamauchi, "Breaking the 10 nm barrier in hard-X-ray focusing," Nat. Phys. **6**(2), 122–125 (2010).
13. J. M. Rodenburg, A. C. Hurst, A. G. Cullis, B. R. Dobson, F. Pfeiffer, O. Bunk, C. David, K. Jefimovs, and I. Johnson, "Hard-X-Ray lensless imaging of extended objects," Phys. Rev. Lett. **98**(3), 034801 (2007).
14. P. Thibault, M. Dierolf, A. Menzel, O. Bunk, C. David, and F. Pfeiffer, "High-resolution scanning x-ray diffraction microscopy," Science **321**(5887), 379–382 (2008).

#184683 - $15.00 USD Received 1 Feb 2013; revised 30 Mar 2013; accepted 2 Apr 2013; published 8 Apr 2013

15. M. Dierolf, A. Menzel, P. Thibault, P. Schneider, C. M. Kewish, R. Wepf, O. Bunk, and F. Pfeiffer, "Ptychographic X-ray computed tomography at the nanoscale," Nature **467**(7314), 436–439 (2010).
16. Y. Nishino, Y. Takahashi, N. Imamoto, T. Ishikawa, and K. Maeshima, "Three-dimensional visualization of a human chromosome using coherent X-ray diffraction," Phys. Rev. Lett. **102**(1), 018101 (2009).
17. R. Neutze, R. Wouts, D. van der Spoel, E. Weckert, and J. Hajdu, "Potential for biomolecular imaging with femtosecond X-ray pulses," Nature **406**(6797), 752–757 (2000).
18. R. Signorato, O. Hignette, and J. Goulon, "Multi-segmented piezoelectric mirrors as active/adaptive optics components," J. Synchrotron Radiat. **5**(3), 797–800 (1998).
19. J. Susini, D. Labergerie, and L. Zhang, "Compact active/adaptive x-ray mirror: Bimorph piezoelectric flexible mirror," Rev. Sci. Instrum. **66**(2), 2229 (1995).
20. P. Kirkpatrick and A. V. Baez, "Formation of optical images by x-Rays," J. Opt. Soc. Am. **38**(9), 766–774 (1948).
21. T. Kimura, S. Handa, H. Mimura, H. Yumoto, D. Yamakawa, S. Matsuyama, K. Inagaki, Y. Sano, K. Tamasaku, Y. Nishino, M. Yabashi, T. Ishikawa, and K. Yamauchi, "Wavefront control system for phase compensation in hard x-ray optics," Jpn. J. Appl. Phys. **48**(7), 072503 (2009).
22. H. Nakamori, S. Matsuyama, S. Imai, T. Kimura, Y. Sano, Y. Kohmura, K. Tamasaku, M. Yabashi, T. Ishikawa, and K. Yamauchi, "Experimental and simulation study of undesirable short-period deformation in piezoelectric deformable x-ray mirrors," Rev. Sci. Instrum. **83**(5), 053701 (2012).
23. T. Kimura, H. Mimura, S. Handa, H. Yumoto, H. Yokoyama, S. Imai, S. Matsuyama, Y. Sano, K. Tamasaku, Y. Komura, Y. Nishino, M. Yabashi, T. Ishikawa, and K. Yamauchi, "Wavefield characterization of nearly diffraction-limited focused hard x-ray beam with size less than 10 nm," Rev. Sci. Instrum. **81**(12), 123704 (2010).
24. S. Matsuyama, H. Yokoyama, R. Fukui, Y. Kohmura, K. Tamasaku, M. Yabashi, W. Yashiro, A. Momose, T. Ishikawa, and K. Yamauchi, "Wavefront measurement for a hard-X-ray nanobeam using single-grating interferometry," Opt. Express **20**(22), 24977–24986 (2012).
25. H. Yumoto, H. Mimura, T. Koyama, S. Matsuyama, K. Tono, T. Togashi, Y. Inubushi, T. Sato, T. Tanaka, T. Kimura, H. Yokoyama, J. Kim, Y. Sano, Y. Hachisu, M. Yabashi, H. Ohashil, H. Ohmori, T. Ishikawa, and K. Yamauchi, "Focusing of X-ray free-electron laser pulses with reflective optics," Nat. Phys. **7**, 43–47 (2012).
26. C. Song, R. Bergstrom, D. Ramunno-Johnson, H. Jiang, D. Paterson, M. D. de Jonge, I. McNulty, J. Lee, K. L. Wang, and J. Miao, "Nanoscale imaging of buried structures with elemental specificity using resonant x-ray diffraction microscopy," Phys. Rev. Lett. **100**(2), 025504 (2008).
27. Y. Takahashi, H. Kubo, H. Furukawa, K. Yamauchi, E. Matsubara, T. Ishikawa, and Y. Nishino, "Element-specific hard x-ray diffraction microscopy," Phys. Rev. B **78**(9), 092105 (2008).
28. M. Shimura, A. Saito, S. Matsuyama, T. Sakuma, Y. Terui, K. Ueno, H. Yumoto, K. Yamauchi, K. Yamamura, H. Mimura, Y. Sano, M. Yabashi, K. Tamasaku, K. Nishio, Y. Nishino, K. Endo, K. Hatake, Y. Mori, Y. Ishizaka, and T. Ishikawa, "Element array by scanning X-ray fluorescence microscopy after *cis*-diamminedichloro-platinum(II) treatment," Cancer Res. **65**(12), 4998–5002 (2005).
29. S. Matsuyama, H. Mimura, H. Yumoto, Y. Sano, K. Yamamura, M. Yabashi, Y. Nishino, K. Tamasaku, T. Ishikawa, and K. Yamauchi, "Development of scanning x-ray fluorescence microscope with spatial resolution of 30," Rev. Sci. Instrum. **77**(10), 103102 (2006).
30. S. Matsuyama, H. Mimura, H. Yumoto, K. Yamamura, Y. Sano, K. Endo, Y. Mori, Y. Nishino, K. Tamasaku, T. Ishikawa, M. Yabashi, and K. Yamauchi, "Diffraction-limited two-dimensional hard-x-ray focusing at the 100 nm level using a Kirkpatrick-Baez mirror arrangement," Rev. Sci. Instrum. **76**(8), 083114 (2005).
31. B. Abbey, K. A. Nugent, G. J. Williams, J. N. Clark, A. G. Peele, M. A. Pfeifer, M. de Jonge, and I. McNulty, "Keyhole coherent diffractive imaging," Nat. Phys. **4**(5), 394–398 (2008).
32. S. Morishita, J. Yamasaki, K. Nakamura, T. Kato, and N. Tanaka, "Diffractive imaging of the dumbbell structure in silicon by spherical-aberration-corrected electron diffraction," Appl. Phys. Lett. **93**(18), 183103 (2008).
33. J. Miao, D. Sayre, and H. N. Chapman, "Phase retrieval from the magnitude of the Fourier transforms of nonperiodic objects," J. Opt. Soc. Am. A **15**(6), 1662–1669 (1998).
34. J. R. Fienup, "Phase retrieval algorithms: a comparison," Appl. Opt. **21**(15), 2758–2769 (1982).
35. H. M. Quiney, A. G. Peele, Z. Cai, D. Paterson, and K. A. Nugent, "Diffractive imaging of highly focused X-ray fields," Nat. Phys. **2**(2), 101–104 (2006).
36. H. Yumoto, H. Mimura, S. Matsuyama, S. Handa, Y. Sano, M. Yabashi, Y. Nishino, K. Tamasaku, T. Ishikawa, and K. Yamauchi, "At-wavelength figure metrology of hard x-ray focusing mirrors," Rev. Sci. Instrum. **77**(6), 063712 (2006).
37. G. R. Brady and J. R. Fienup, "Nonlinear optimization algorithm for retrieving the full complex pupil function," Opt. Express **14**(2), 474–486 (2006).

1. Introduction

X-ray microscopy has made significant advances over the last decade, and is widely used in nanoscale imaging [1–3]. Coherent x-ray imaging techniques, such as coherent x-ray diffraction microscopy [4,5], are also of growing importance [6]. However, most x-ray microscopy methods lack a zoom function, although it is critically important for wider application of the technology. There have been some examples of zooming technology in x-ray microscopy, *e.g.* use of a divergent x-ray beam [7] and an x-ray imaging detector with a

#184683 - $15.00 USD Received 1 Feb 2013; revised 30 Mar 2013; accepted 2 Apr 2013; published 8 Apr 2013

zooming function [8], but they are only applicable to specific x-ray imaging modalities. For compatibility with a range of x-ray imaging modalities, it is desirable to have x-ray optics that can deliver a coherent x-ray beam with controllable focal spot size at a fixed focal position. In this study, we propose a zoom condenser lens for coherent x-rays, and show how this lens can be applied to imaging on diverse length scales.

The proposed zoom condenser lens is composed of two-stage deformable Kirkpatrick-Baez (KB) mirrors. The lens maintains diffraction-limited focusing, which is ideal for coherent x-ray diffraction microscopy [9–11]. The zoom condenser lens can control the focal spot size at a fixed focal position, and this feature simplifies microscopy-based measurement considerably; we can easily zoom in on regions of interest in samples in both coherent x-ray diffraction microscopy and scanning x-ray microscopy. By extending our previous studies to achieve sub-10 nm x-ray focusing with an adaptive mirror [12], we intend to control the numerical aperture of the mirror system by using piezoelectric bimorph mirrors.

We also propose a new coherent x-ray diffraction microscopy scheme, called apodized-illumination coherent x-ray diffraction microscopy, to image regions of interest in extended objects from a single coherent diffraction pattern. The scheme uses an apodized focused beam produced by the coherent x-ray zoom condenser lens with a spatial filter. Although coherent diffraction microscopy usually requires a scanning method called ptychography to image spatially-extended objects [13–15], the apodized-illumination scheme can image part of an extended object without the need to scan the sample position. The new scheme will be suitable for a number of important applications. For example, the non-scanning feature will lead to highly efficient measurement with ultimate storage ring sources, and is beneficial, e.g., for three-dimensional bioimaging [15,16]. The new scheme will also enable single-shot imaging of extended objects with x-ray free electron lasers (XFELs) [17], where the destructively high photon density of the focused XFEL prevents the application of ptychography.

2. Coherent x-ray zoom condenser lens

2.1 Optical design

The diffraction-limited focal spot size w for a probe with a wavelength λ is generally expressed as

$$w \approx \frac{\lambda}{2NA} \tag{1}$$

for focusing optics with a rectangular aperture. To control the focal spot size with a fixed wavelength, focusing optics with variable numerical aperture NA are thus required. Here, the numerical aperture NA is given by

$$NA \approx \frac{a}{2f_b}. \tag{2}$$

where f_b is the back focal length and a is the aperture size of the focusing optics. When the beam size at the focusing optics is smaller than the aperture of the focusing optics, then a is effectively given by the beam size. For focusing mirrors, a is given by $a \approx L \sin\theta$, where θ is the grazing incidence angle and L is the mirror length. Because the critical angle for x-ray total-reflection is small, and is typically of the order of mrad for hard x-rays, it is unrealistic to try to enhance the numerical aperture by increasing θ.

One method that is widely used to control the numerical aperture is the use of deformable mirrors, which change f_b in Eq. (2) [18,19]. In this case, the focal position inevitably moves, although ideally for microscopy, the focal position should be maintained while the focal spot size changes. In addition, to our knowledge it has not been realized to change NA of the mirrors while keeping the diffraction-limited focusing condition. Another way to change the numerical aperture is to place an aperture-limiting slit just before the focusing mirror to

#184683 - $15.00 USD Received 1 Feb 2013; revised 30 Mar 2013; accepted 2 Apr 2013; published 8 Apr 2013

effectively control the aperture size a in Eq. (2). With narrower slits, the focal spot size increases with smaller NA, but this method is associated with a decrease in the focused beam intensity, leading to lower focusing efficiency. Ideally, the full incident flux should be used for high focusing efficiency.

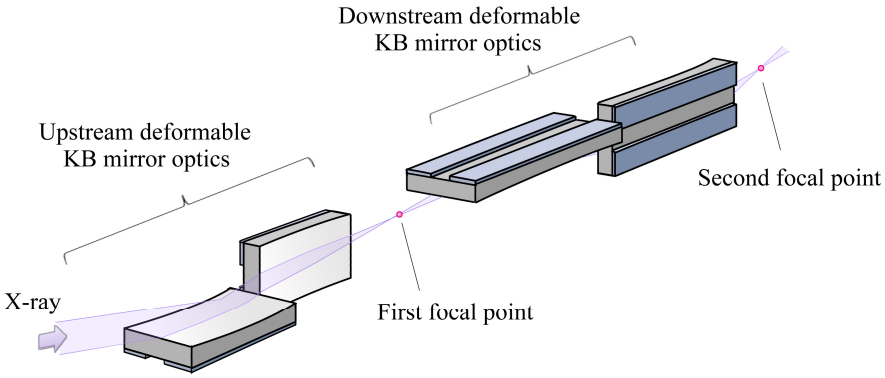

Fig. 1. Schematic of coherent x-ray zoom condenser lens composed of two-stage deformable KB mirrors. The upstream and downstream KB mirrors share a single focus at the first focal point. The second focal spot size can be controlled at a fixed focal position by adjusting the first focal position.

To overcome these problems, we propose a two-stage deformable KB mirror system, as shown schematically in Fig. 1. In the upstream KB mirror system, the front focal position is fixed at the source, and the back focal position (the first focal position) moves between the two deformable mirrors. In the downstream KB mirror system, the front focal position is controlled to coincide with the first focal position, and the back focal position (the second focal position) is fixed at the sample. The proposed optical system is similar to that of the two-stage zoom condenser lens that is widely used in scanning electron microscopes.

Figure 2 illustrates how the optics works, for simplicity, for one-dimensional focusing. The numerical aperture NA of the entire optical system is controlled by moving the first focal position. When the first focal position is closer to the second mirror, then a smaller portion of the second mirror is illuminated. Accordingly, the NA becomes smaller, and a larger focal spot size is achieved. Conversely, when the first focal position is further away from the second mirror, a larger proportion of the second mirror is illuminated. Accordingly, the NA increases, and a smaller focal spot size is achieved. The smallest focal spot size is achieved when the beam size at the second mirror coincides with the aperture size of the second mirror. This condition thus determines the furthest distance that the first focus can be from the second mirror. If the first focus is further from the second mirror than the distance determined by this condition, the beam size at the second mirror then becomes greater than the aperture size of the second mirror. In this case, the focal spot size will not improve but the system will suffer from decreased focusing efficiency. Making the second mirror larger than the first mirror will therefore help to secure a wider focal spot size range.

The numerical aperture NA of the entire optical system is expressed as

$$NA = NA_1 \frac{f_{f2}}{f_{b2}} = \frac{a f_{f2}}{2 f_{b1} f_{b2}} = \frac{a f_{f2}}{2(D - f_{f2}) f_{b2}}, \tag{3}$$

where NA_1, f_{b1}, f_{f2}, and f_{b2} are the numerical aperture of the upstream mirror, the back focal length of the upstream mirror, and the front and back focal lengths of the downstream mirror, respectively. D is the distance between the two mirrors, which is equal to the sum of f_{b1} and f_{f2}. Because a and f_{b2} are fixed in our case, Eq. (3) shows that the NA is proportional to $f_{f2}/(D$-

#184683 - $15.00 USD Received 1 Feb 2013; revised 30 Mar 2013; accepted 2 Apr 2013; published 8 Apr 2013

f_{f2}). Therefore, the spot size at the second focus can be controlled by adjusting f_{f2}, while the second focal position is fixed.

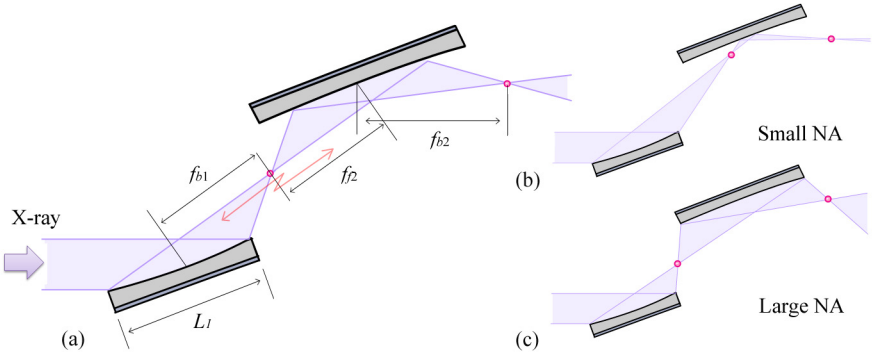

Fig. 2. Schematic of the zooming mechanism. For simplicity, the figure is drawn to show one-dimensional focusing. (a) The positions of the second focus and the source are fixed, while the first focal position can be controlled on demand. (b) When the first focal position is closer to the second mirror, a larger focal spot size can be achieved with a smaller *NA*. (c) Conversely, when the first focal position is further away from the second mirror, a smaller focal spot size can be achieved with a larger *NA*.

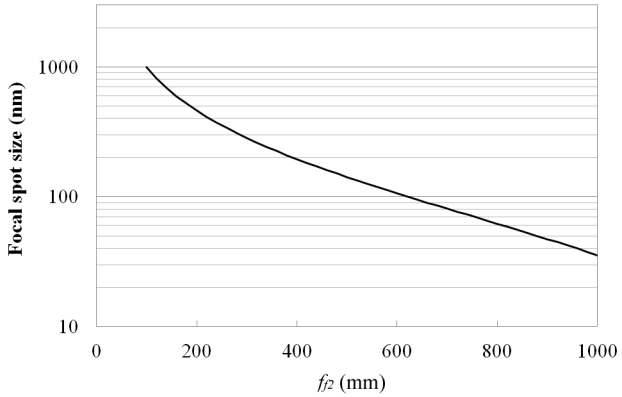

Fig. 3. Dependence of the focal spot size on the first focal position. The curve is obtained by using Eqs. (1) and (3) with a = 350 μm, D = 1.5 m, and f_{b2} = 200 mm for 10 keV x-rays. The focal spot size can be controlled over a wide range, from one micrometer to a few tens of nanometers, with these realizable parameters.

To illustrate how the focal spot size changes with the first focal position, Fig. 3 shows the results of calculations based on Eqs. (1) and (3) with the following parameters as a realistic example: an x-ray photon energy of 10 keV, an effective beam size of a = 350 μm, a distance between the two mirrors of D = 1.5 m, and a back focal length for the downstream mirror of f_{b2} = 200 mm. The operating range for the front focal length f_{f2} of the downstream mirror was set to be between 100 mm and 1000 mm, assuming that the second mirror is two times longer than the first mirror. The calculation results depicted in Fig. 3 show that our optics with these realistic parameters can control the focal spot size of a coherent x-ray beam from one micrometer to a few tens of nm with a fixed focal position.

2.2 Requirements for wavefront control

The focal spot size calculated above can be achieved for diffraction-limited focusing, where the unwanted wavefront distortion caused by the focusing optics is negligible. In diffraction-

#184683 - $15.00 USD Received 1 Feb 2013; revised 30 Mar 2013; accepted 2 Apr 2013; published 8 Apr 2013

limited focusing, the x-ray waves interfere constructively at the focus to form a main lobe with a parallel wavefront. Diffraction-limited focusing is ideal for coherent x-ray diffraction microscopy, because it helps to minimize the parasitic scattering from the focusing optics and allows us to measure the coherent diffraction pattern with a high signal-to-noise ratio.

To achieve diffraction-limited focusing, the wavefront profile must be controlled with an accuracy of better than $\lambda/4$ to satisfy Rayleigh's quarter wavelength rule. For total reflection mirrors, a surface height difference of δ produces a light path difference of $2\delta \sin\theta$, where θ is the grazing incidence angle. Rayleigh's quarter wavelength rule therefore requires

$$\delta < \frac{\lambda}{8\sin\theta}. \tag{4}$$

For total x-ray reflection, the maximum grazing incidence angle is given by the critical angle θ_c, and is expressed as

$$\theta_c = \lambda\sqrt{\frac{n_a r_e f_1(\lambda)}{\pi}} \approx \lambda\sqrt{\frac{n_e r_e}{\pi}}. \tag{5}$$

Here, r_e is the classical electron radius, f_1 is the real part of the atomic scattering factor for forward scattering, n_a is the atom number density, and n_e is the electron number density [20]. In the approximate equality of Eq. (5), we have assumed that the wavelength is not close to any absorption edge. Equations (4) and (5) can be combined to give

$$\delta < \frac{1}{8}\sqrt{\frac{\pi}{n_e r_e}}. \tag{6}$$

Equation (6) implies that the requirement for the surface accuracy of an x-ray total reflection mirror is determined solely by the electron number density n_e of the mirror material, and that higher surface precision is thus required for mirrors with higher electron number densities. For silicon, $n_e = 0.7$ $e^-/Å^3$ and Eq. (6) gives $\delta<5.0$ nm. For platinum, as an example of a high n_e material, $n_e = 5.2$ $e^-/Å^3$ and $\delta<1.8$ nm.

We have already developed deformable wavefront-compensation mirrors that can control their surface profiles with an accuracy of less than one nanometer [12], which is sufficient to meet the Rayleigh quarter wavelength rule for any mirror material. The high-precision flat surface of the deformable mirrors was fabricated by elastic-emission machining after attaching piezoelectric elements to the back face of the mirror substrate [21,22]. For high-precision control of the mirror deformation, the mirror surface figure was determined by applying an iterative phase retrieval algorithm to the measured intensity profiles in a series of planes near the focal plane. The accuracy of retrieved phases was demonstrated to be $\sim\lambda/12$, which is much better than is required by Rayleigh's quarter wavelength rule [23].

When the x-ray zoom condenser lens is used as beamline optics, focal spot size should be changed speedy during beamtime. To achieve this, optimum parameters for different focal spot sizes, such as voltages to be applied to piezoelectric elements, should be determined in advance at the commissioning stage. Measurement to determine optimum parameters can be performed efficiently using recently developed single-grating interferometry [24]. Single-grating interferometry can determine the mirror surface figure from a single Talbot interferogram. Once a parameter table for different focal spot sizes is made, it would be straightforward to achieve desired focal spot size with well-reproducible optical system, in principle. In addition, quick check of focusing condition and the mirror figure can be performed during beamtime using single-grating interferometry.

2.3 Application of coherent x-ray zoom condenser lens to microscopy

The coherent x-ray zoom condenser lens is suitable for use in permanently installed beamline optics in storage ring and XFEL facilities. Users simply mount the sample at a fixed position,

#184683 - $15.00 USD Received 1 Feb 2013; revised 30 Mar 2013; accepted 2 Apr 2013; published 8 Apr 2013

and the optics can then deliver a coherent x-ray beam with the desired beam size on demand. It is beneficial to have focusing optics that are capable of providing the versatile imaging modalities on diverse length scales, that can be realized with this lens. The high radiation hardness of the x-ray total reflection mirrors is preferable for applications at XFEL facilities [25].

The coherent x-ray zoom condenser lens can optimize the probe beam size for each measurement, and this is an important parameter in microscopy. In scanning x-ray microscopy, the probe beam size usually determines the spatial resolution. For coherent x-ray diffraction microscopy for single isolated sample particles, it is best to tune the probe beam size to be a little larger than the sample size to achieve the maximum x-ray flux density at the sample position for efficient measurement.

The achromaticity of the x-ray total reflection mirror is also beneficial for high-precision x-ray photon energy scanning in, *e.g.* micro-x-ray absorption near-edge spectroscopy measurements, and also for element-specific coherent x-ray diffraction microscopy using anomalous x-ray scattering [26,27].

It is envisaged that the coherent x-ray zoom condenser lens can be used for novel x-ray microscopy methods that combine diffractive microscopy with various types of scanning x-ray microscopy [2,28,29]. Figure 4 shows an example experimental setup. This experimental setup allows us to obtain a variety of information from the sample, and can easily zoom in on regions of interest. For example, it allows us to image many samples at low resolution for screening and then perform high-resolution imaging for the most promising samples within the limited beamtime allocated.

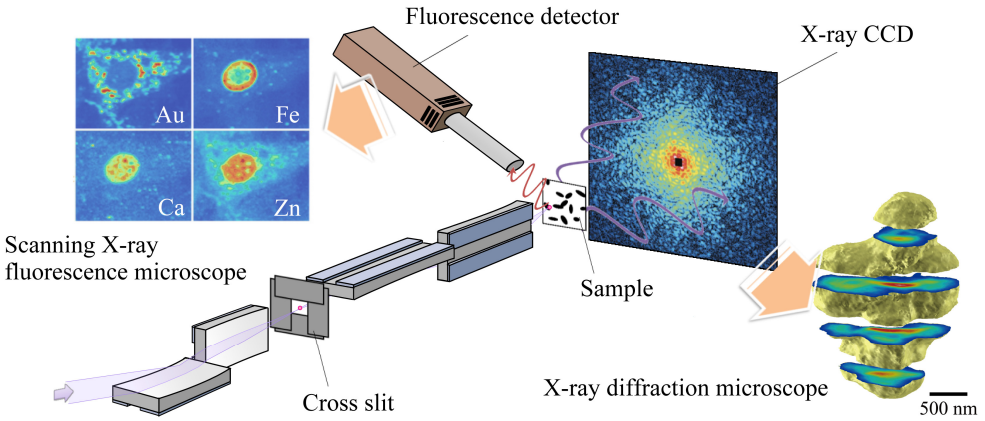

Fig. 4. Example experimental setup for novel x-ray microscopy using the coherent x-ray zoom condenser lens. Coherent x-ray diffraction microscopy and various types of scanning x-ray microscopy can be combined in a single experimental setup.

3. Apodized-illumination coherent x-ray diffraction microscopy

We also propose non-scanning coherent x-ray diffraction microscopy for spatially-extended objects by using an apodized and focused beam produced by the coherent x-ray zoom condenser lens with a spatial filter. We refer to the proposed scheme as apodized-illumination coherent diffraction microscopy.

In the focusing optics, the intensity distribution in the focal plane generally has side lobes in addition to the main lobe because of the finite aperture of the focusing optics. Although the intensity is mostly concentrated in the main lobe, the side lobes extend to a much wider area than the main lobe. For high precision scanning microscopy, it is best to apodize the focused beam by removing the side lobes, and thus the unwanted signals from the side lobes can be reduced. Apodized illumination can also be applied to ptychography. Furthermore, it can be

#184683 - $15.00 USD Received 1 Feb 2013; revised 30 Mar 2013; accepted 2 Apr 2013; published 8 Apr 2013

also used for non-scanning coherent x-ray diffraction microscopy for spatially-extended objects, as we demonstrate below through a numerical simulation.

For coherent x-ray zoom condenser lenses, the focused beam can be apodized by installing an appropriate spatial filter at the first focus and by making the beam size at the second mirror smaller than the aperture of the second mirror. This method allows us to secure the working space around the sample at the second focus without the need to introduce an aperture just before the sample. We expect that the spatial filter at the first focus will produce much lower parasitic scattering as compared to the case when an aperture is placed just before the sample. The reduction of parasitic scattering is of key importance in coherent x-ray diffraction microscopy, because high-quality coherent diffraction data is essential for faithful reconstruction of sample image. Furthermore, the required aperture positioning accuracy is lower, when the beam size is larger at the first focus than at the second focus.

We performed a wave-optical simulation [30] of the coherent x-ray zoom condenser lens, and calculated the beam profiles with and without a spatial filter. In this simulation, we use the parameters shown in Table 1. The x-ray photon energy was set to 10 keV. A spatial filter was positioned at the first focus to allow only the main peak to pass. The intensity distributions at the first focus with and without the spatial filter are shown in Fig. 5(a) and 5(b), respectively. The intensity distributions at the second focus with and without the spatial filter are shown in Fig. 5(c) and 5(d), respectively. As clearly shown in the figures, the side lobe intensities at the second focal plane are reduced considerably by the introduction of the spatial filter at the first focal plane. To display the intensity decrease of the side lobes more quantitatively, Fig. 5(e) shows the intensity profiles in the vertical direction through the second focal plane. The intensity ratio between the main peak and the first satellite peak decreased from 4.0% to 0.093% after introduction of the spatial filter.

Table 1. Parameters used in the simulation of the two-stage deformable KB mirror optics

	Upstream KB mirror system		Downstream KB mirror system	
	Mirror 1	Mirror 2	Mirror 3	Mirror 4
Mirror length	75 mm	75 mm	150 mm	150 mm
Grazing incidence angle	3.6 mrad	3.6 mrad	3.6 mrad	3.6 mrad
Front focal length	45 m	45.1 m	350 mm	455 mm
Back focal length	1150 mm	1050 mm	255 mm	150 mm

Using the wave-optically simulated focused beam for the sample illumination, we then performed a simulation of coherent diffraction microscopy for a spatially-extended sample. The extended sample image used for the simulation is shown in Fig. 6(a). Figures 6(b) and 6(c) show the wave amplitudes in the sample exit plane with and without the spatial filter, respectively, which were obtained by multiplying Fig. 6(a) by the simulated focused beam amplitudes. With the apodized illumination produced by the spatial filter, the wave amplitude in the exit plane becomes nearly isolated, as shown in Fig. 6(b). The nearly isolated wave amplitude at the sample exit plane helps us to define a support (non-zero amplitude region) in image reconstruction, as described below. The idea of using confined illumination that was applied here to non-scanning coherent diffraction microscopy for extended objects was also used in keyhole coherent diffractive imaging [31], where the sample is illuminated with a divergent beam, and in selected-area coherent electron diffraction microscopy [32].

#184683 - $15.00 USD Received 1 Feb 2013; revised 30 Mar 2013; accepted 2 Apr 2013; published 8 Apr 2013

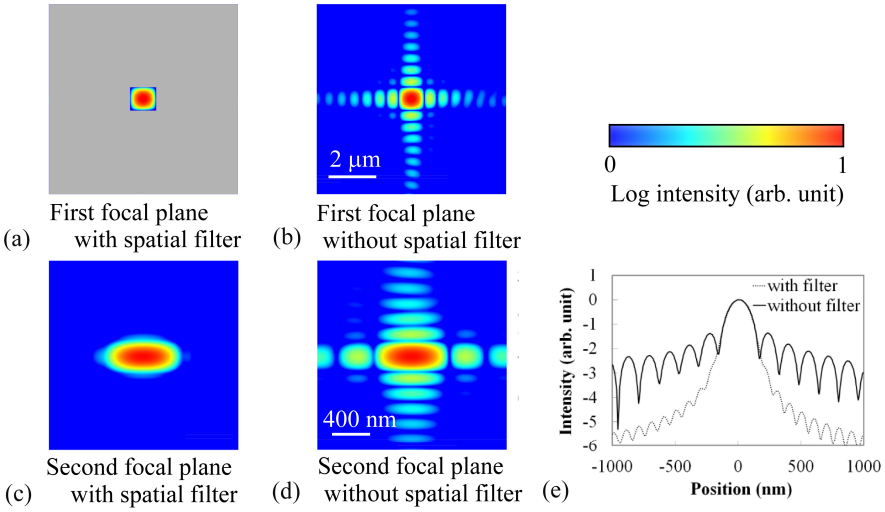

Fig. 5. Intensity distributions at the two focal planes. Intensity distributions at the first focal plane are shown (a) with the spatial filter and (b) without the spatial filter. Intensity distributions at the second focal plane are shown (c) with the spatial filter and (d) without the spatial filter. (e) Intensity profiles are compared in the vertical direction through the second focus.

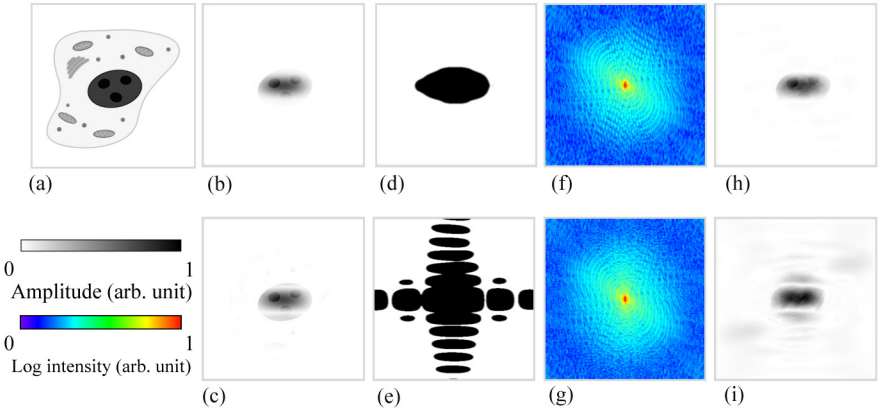

Fig. 6. Simulation of apodized-illumination coherent diffraction microscopy. (a) Spatially-extended sample image used for the simulation. The remaining parts of the figure show the results with and without the spatial filter, respectively: (b) and (c) are the amplitudes of the exit wave; (d) and (e) are the supports for the hybrid input-output algorithm; (f) and (g) are the simulated coherent diffraction patterns; and (h) and (i) are the reconstructed images.

We set the support region for image reconstruction to be the region where the illuminating x-ray intensity is higher than 0.1% of the peak in each case with or without the spatial filter, and the support regions defined in this way are shown in Figs. 6(d) and 6(e). Because the support without the spatial filter, Fig. 6(e), extends out to the edge of real space, scattering from larger area than is accounted for in this simulation will give non-negligible contribution in actual measurement. Considering that the speckle size in coherent diffraction pattern is inversely proportional to the scattering area, this implies that without the spatial filter the speckle becomes smaller and difficult to be resolved with the detector. Therefore, the confined support achieved by the spatial filter, Fig. 6(d), is advantageous for image reconstruction in coherent diffraction microscopy.

#184683 - $15.00 USD Received 1 Feb 2013; revised 30 Mar 2013; accepted 2 Apr 2013; published 8 Apr 2013

The ratios of the support area to the total area are 7.87% and 30.1% for Figs. 6(d) and 6(e), respectively. Inverse of these values correspond to the oversampling ratio in two dimensions. The oversampling condition requires that the oversampling ratio should be larger than two [33], and both Figs. 6(d) and 6(e) satisfy this condition. However, in practices, lager oversampling ratio makes image reconstruction easier because of larger amount of real-space constraints.

Figures 6(f) and 6(g) show the calculated coherent diffraction patterns with and without the spatial filter, respectively. We then apply the hybrid input-output (HIO) algorithm [34] to the coherent diffraction patterns to reconstruct the sample image. We performed 10000 HIO iterations using the support for each case starting from 12 different random seeds, and the ten most similar images were averaged to obtain the final reconstruction. Figures 6(h) and (i) show the results of image reconstruction with and without the spatial filter, respectively. The reconstruction results with the spatial filter in Fig. 6(h) successfully show a good agreement with the exit-wave amplitude shown in Fig. 6(b), while the reconstruction without the spatial filter was unsuccessful, as shown in Fig. 6(i). To evaluate the reconstruction quality quantitatively, the root mean square errors of the reconstructed images as compared to the exit wave amplitude improved by a factor of 1.5 after introduction of the spatial filter.

The results of our simulation show the great potential of apodized-illumination coherent x-ray diffraction microscopy for reconstruction of spatially-extended objects from a single coherent diffraction pattern without the need to scan the sample position. This also enables a new way to perform coherent diffraction microscopy for extended objects with XFELs, where the destructively high pulse intensity does not allow us to perform ptychography. The efficient non-scanning scheme will also be helpful in a number of applications with storage ring sources including three-dimensional imaging, bioimaging with low radiation doses, and cryo-bioimaging with reduced effects from contamination accumulation on the sample surface. For determination of illuminating X-ray wave field in these experiments, iterative phase retrieval methods [23,35–37] or single-grating interferometry [24] can be used. Single-grating interferometry is especially advantageous with XFELs, because interferograms needed to determine illuminating X-ray wave field can be measured with a sing-shot of XFELs.

4. Conclusion

We have proposed a coherent x-ray zoom condenser lens composed of two-stage deformable KB mirrors. The lens controls the coherent x-ray beam size at a fixed focal position. Using a realistic parameter set, we showed that the coherent x-ray beam size can be controlled in a range from one micrometer to a few tens of nanometers. We also showed that the required precision for diffraction-limited focusing can be achieved with the existing deformable mirror technologies that are used for sub-10 nm focusing.

The coherent x-ray zoom condenser lens can be applied to a novel x-ray microscopy method that combines diffractive microscopy with various types of scanning x-ray microscopy. Apodized illumination produced by using a coherent x-ray zoom condenser lens with an appropriate spatial filter at the first focal plane can be used for high-precision scanning microscopy. We also proposed apodized-illumination coherent x-ray diffraction microscopy, which allows us to image spatially-extended objects without the need to scan the sample position. Apodized-illumination coherent x-ray diffraction microscopy will enable single-shot diffraction microscopy to be performed for extended objects with XFELs, and will also play an important role in efficient imaging with ultimate storage ring sources.

Acknowledgments

This study was supported by CREST (JST); KAKENHI (JSPS) Grant Numbers 23860001, 22310075, 23651126, 23710128, and 23226004; the X-ray Free-Electron Laser Priority Strategy Program (MEXT); and the Cooperative Research Program of “Network Joint Research Center for Materials and Devices”.